Charge disproportionation of Mn 3d and O 2p electronic states depending on strength of p-d hybridization in (LaMnO_{3})_{2}(SrMnO_{3})_{2} superlattices

Hironori Nakao, Chihiro Tabata, Youichi Murakami, Yuichi Yamasaki, Hiroyuki Yamada, Sumio Ishihara, and Masashi Kawasaki

Phys. Rev. B **98**, 245146 — Published 26 December 2018

DOI: 10.1103/PhysRevB.98.245146

Charge disproportionation of Mn $3d$ and O $2p$ electronic states depending on strength of the p-d hybridization in $(LaMnO_3)_2(SrMnO_3)_2$ superlattices

Hironori Nakao,* Chihiro Tabata,† and Youichi Murakami
Condensed Matter Research Center and Photon Factory, Institute of Materials Structure Science, High Energy Accelerator Research Organization (KEK), Tsukuba 305-0801, Japan

Yuichi Yamasaki
National Institute for Materials Science (NIMS), Tsukuba 305-0047, Japan and RIKEN Center for Emergent Matter Science (CEMS), Wako 351-0198, Japan

Hiroyuki Yamada
National Institute of Advanced Industrial Science and Technology (AIST), Tsukuba 305-8565, Japan

Sumio Ishihara
Department of Physics, Tohoku University, Sendai 980-8578, Japan

Masashi Kawasaki
RIKEN Center for Emergent Matter Science (CEMS), Wako 351-0198, Japan and Department of Applied Physics and Quantum-Phase Electronics Center (QPEC), University of Tokyo, Tokyo 113-8656, Japan

(Dated: December 10, 2018)

The charge disproportionation of Mn $3d$ and O $2p$ electronic states was investigated in two $(LaMnO_3)_2(SrMnO_3)_2$ superlattices using the resonant x-ray scattering technique. The superlattices show significantly different conductivity even though the same composition. The large modulation of the Mn $3d$ electronic state was observed in the insulating sample, however the charge disproportionation and magnetic modulation of O $2p$ were shown in the semiconductive sample. It is suggested that the charge modulation appears in either Mn $3d$ or O $2p$, which is strongly related with strength of the p-d hybridization, is the main factor determining the electric conductivity in the superlattices.

INTRODUCTION

Metal-insulator transition (MIT) is one of the important phenomena in transition metal oxides, and various intriguing physical properties, such as high T_C superconductivity and colossal magnetoresistance effects, appear close to MIT [1]. Here, bandwidth dominates the localized and itinerant character in materials [2]. Perovskite nickelate, RNiO$_3$, is a typical compound that exhibits charge-transfer type MIT [3]. Bandwidth is controlled by the Ni-O-Ni bond angle, which reflects orthorhombic distortion, i.e., the tolerance factor. The strength of the orbital hybridization between Ni $3d$ and O $2p$ is directly connected to bandwidth. Two kinds of charge orderings have been proposed theoretically in the insulating phase [4], even though it is still under debates in perovskite nickelate. In the case of narrow bandwidth, charge ordering occurs at the Ni site, $2Ni^{3+} \rightarrow Ni^{2+} + Ni^{4+}$. In contrast, in the case of wider bandwidth, all Ni ions are Ni^{3+}, while oxygen sites show the charge disproportionation of the O $2p$ electron. This proposal indicates that the charge disproportionation of Ni $3d$ and O $2p$ is dominated by the degree of the orbital hybridization between Ni $3d$ and O $2p$. However, since it is difficult to distinguish experimentally these two kinds of charge ordering, the hybridized state of Ni $3d$ and O $2p$ becomes a hidden parameter in the insulating phase of RNiO$_3$.

The manganite superlattice, $(LaMnO_3)_m(SrMnO_3)_n$ (LmSn), has been extensively investigated as a stage to control Mn valence, as the Mn valences in the $LaMnO_3$ (LMO) and the $SrMnO_3$ (SMO) layers are 3+ and 4+, respectively [5–13]. Namely the charge modulation is controlled by the A-site cations; that is different from the charge ordering in RNiO$_3$. The physical properties of the LmSn superlattice strongly depend on the stacking structure of the LMO and SMO layers [5–7]. In addition, a large negative magnetoresistance has been newly discovered [8, 10]. In this study, we focus on two L2S2 superlattices, here we refer to them as sample 1 and 2, in which conductivities have been reported to be dependent on samples [7]. The temperature profiles of resistivity in two L2S2 samples are shown in Fig. 1(a). The resistivity of sample 2 is considerably smaller than that of sample 1, even though both samples show semiconducting behavior. X-ray diffraction elucidated that the accuracy of stacking in sample 1 are better than that in sample 2 [7] (Fig. 2). The suppression of charge disproportionation owing to the mixing of La and Sr had been simply expected to be a cause of resistivity reduction.

Resonant x-ray scattering (RXS) is a powerful tool for observing the spatial ordering of the charge, orbital, and spin degrees of freedom [14, 15]. A resonant signal con-

sists of element and orbital selective information depending on absorption energy. Hence, the Mn valence distribution of the L2S2 superlattices was evaluated using RXS at the Mn K edge [7]. However, RXS spectra were almost same in two L2S2 samples. Namely, the difference in Mn valence distribution could not be detected within experimental accuracy, and it was elucidated that Mn valences are fully ordered as shown in Fig. 1(c). The RXS signal at the Mn K edge directly reflects the $4p$ electronic state of the Mn ion because the edge corresponds to the $1s \rightarrow 4p$ transition. The $4p$ electronic state shows an energy shift that reflects the valence state (chemical shift). Therefore, we consider that the chemical shift is not very sensitive to the difference between the charge disproportionation of Mn $3d$ and O $2p$. As a result, it is difficult to distinguish this kind of charge disproportionation by utilizing the RXS signal at the Mn K edge.

In the present study, we consider the charge disproportionation of Mn $3d$ and O $2p$, which is expected to influence conductivity properties through the orbital hybridization between Mn $3d$ and O $2p$. Namely, the charge disproportionation of O $2p$ is enhanced by the orbital hybridization in sample 2. In this Letter, we describe the RXS measurements performed not only at the Mn $L_{2,3}$ edge but also at the O K edge to elucidate atypical charge modulations because the RXS at the Mn $L_{2,3}$ edge ($2p \rightarrow 3d$ transition) and at O K edge ($1s \rightarrow 2p$ transition) can directly clarify the Mn $3d$ and O $2p$ electronic states, respectively. In fact, the charge and orbital order at the oxygen site have been reported utilizing the RXS at the O K edge [16, 17].

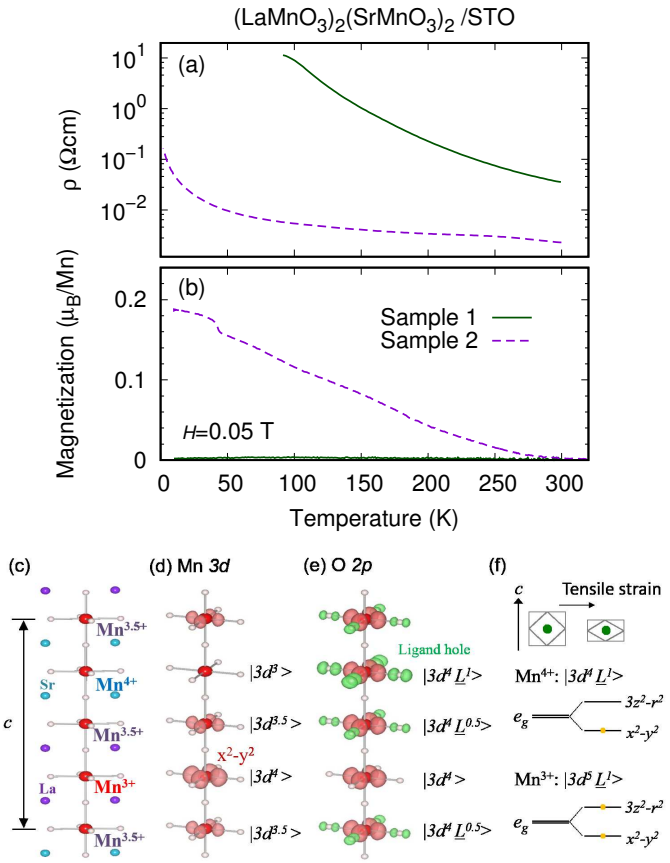

FIG. 1. (Color online) Temperature dependences of (a) resistivity and (b) magnetization [7] for sample 1 and sample 2. Schematic view of (c) crystal structure of the L2S2 superlattice, Charge disproportionation of (d) Mn $3d$ and (e) O $2p$. (f) Energy levels of e_g orbital with a ligand hole under tensile strain.

EXPERIMENTS

The L2S2 superlattice was fabricated on a $SrTiO_3$ (STO) (001) substrate using the pulsed laser deposition technique [18]. The lattice constant, c, along the stacking direction was almost four primitive cells of perovskite (Fig. 1(c)). Magnetization was measured using MPMS (Quantum Design, Inc.). A magnetic field ($H = 0.05$ T) was applied parallel to the in-plane direction.

X-ray diffraction and RXS at the Mn K edge were carried out at BL-3A and BL-4C, Photon Factory (PF), KEK. Experiment was performed on a four-circle diffractometer with σ-polarized x rays at room temperature. RXS experiments were performed close to the Mn $L_{2,3}$ edge and O K edge at BL-19B in PF using an in-vacuum two-circle diffractometer [19, 20]. A π-polarized incident x-ray was used as shown in the inset of Fig. 3(b). Polarization analysis was not performed [21]. Hence, the measured intensity was integrated over π' and σ' final state polarizations.

X-ray magnetic circular dichroism (XMCD) measurement was conducted at BL-16A in PF using a circularly polarized x-ray from APPLE-II type undulators [22, 23]. XMCD spectra were recorded in the total-electron-yield (TEY) mode. X-ray absorption spectroscopy (XAS) measurement at the O K edge was measured by the fluorescence-yield (FY) mode.

RESULTS AND DISCUSSION

Sample characterization

Manganite superlattice $[(LaMnO_3)_m(SrMnO_3)_m]_n$ was carefully fabricated as reported in Ref. [7]. In order to improve the accuracy of the superlattice periodicity, RHEED intensity oscillations were monitored throughout the fabrication. Hence the stacking number of $(LaMnO_3)_m(SrMnO_3)_m$ unit, i.e. n, is known correctly. The stacking number of the sample 1 and 2 are $n = 24$. On the other hand, the accurate control of the superlattice periodicity m was very difficult. Therefore, the estimation of periodicity m is necessary as the sample characterization.

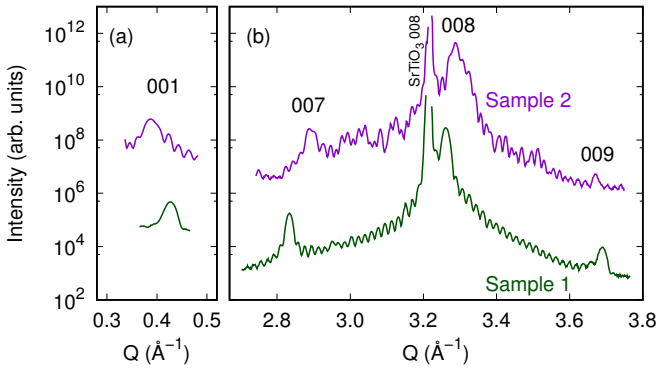

FIG. 2. (Color online) (a) Diffraction patterns near the 001 reflection of Sample 1 (6.52 keV) and Sample 2 (6.50 keV). (b) Those near the 008 reflection observed at 12.0 keV. The base of sample 2 is vertically shifted for clarity.

The diffraction pattern along the stacking direction is shown in Figs. 2. The clear Laue function peaks are observed in sample 1, while the large intensity modulation is observed in the Laue function region of sample 2. The diffraction pattern in Fig. 2(b) almost reproduced previous report (Fig. 16 in Ref. [7]) It indicates that the accuracy of stacking in sample 1 are better than that in sample 2, since the size of deviation from ideal Laue function reflects the stacking accuracy. The peak position of fundamental reflection reflects the lattice constant of average perovskite structure (c_{ave}). Using the peak position of 008 reflection, we estimated the lattice constants, $c_{ave} = 3.85$ Å in sample 1 and $c_{ave} = 3.82$ Å in sample 2, which are consistent with the previous report [7]. The superlattice periodicity m is evaluated by the peak position of the superlattice reflections, 001, 007, and 009. Hence, m is a spatially averaged value, while the Laue function region reflects the whole of structural modulation in film. The estimated m value is about 1.95 in sample 1 and about 2.14 in sample 2, respectively. Hence, the lattice constant, c, along the stacking direction was almost four primitive cells of perovskite. The obtained periodicity m are slightly different from the previous report [7]. It may reflect that the different piece of sample was used in this experiment; The fabricated L2S2 superlattice was cut and one piece was used for previous x-ray measurement [7]. Here, we think that the films have the same characteristics used in previous measurement. In fact, the intensity modulation between the 007 and 008 reflections exactly coincides with that of previous report in the sample 2.

Magnetization was measured to clarify magnetic properties of the L2S2 samples as shown in Fig. 1(b). Spontaneous magnetization was clearly observed in sample 2. This magnetization ($< 0.2\mu_B$/Mn) is considerably smaller than that of ferromagnetic metal samples [6, 8].

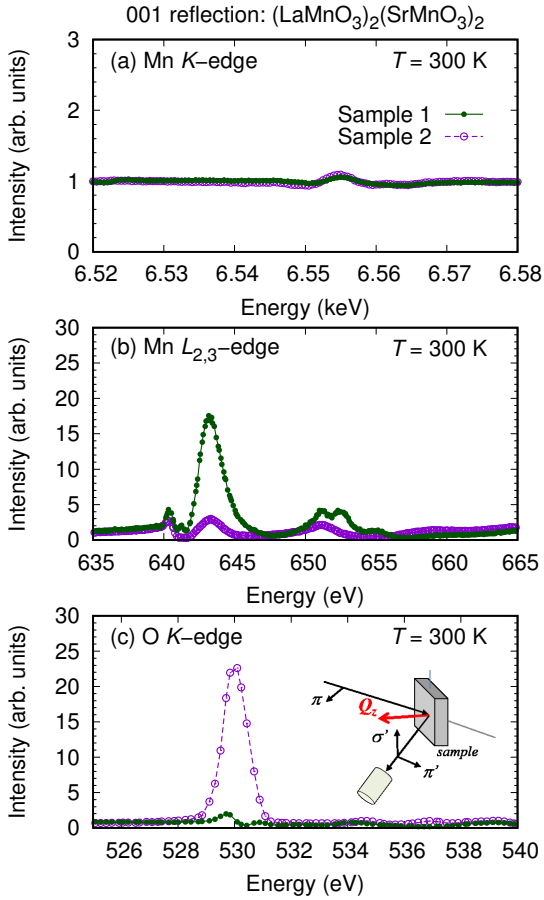

FIG. 3. (Color online) Energy dependence of scattering intensities in the 001 reflection observed at the (a) Mn K edge, (b) Mn $L_{2,3}$ edge and (c) O K edge. Non-resonant intensity scales to 1 through intensity normalization. The diffracted signal is quite strong, and the intensity of the fluorescence is negligible. The inset in (c) shows the schematic view of the experimental configuration.

Moreover, no magnetization was detected in sample 1 within experimental error.

Resonant x-ray scattering

In RXS measurement, scattering intensity $I(E, \vec{Q})$ is proportional to the square of the structure factor, $F(E, \vec{Q})$. $F(E, \vec{Q})$ is expressed as $\sum_j f_j(E, \vec{Q}) \exp(-i\vec{Q} \cdot \vec{r}_j)$, where $f(E, \vec{Q})$ and r_j denote the atomic scattering factor and the atomic position in a unit cell, respectively. The atomic scattering factor is given by $f_0(\vec{Q}) + f'(E) + if''(E)$, where f_0, $f'(E)$, and $f''(E)$ represent the Thomson scattering factor and the real and imaginary terms of the anomalous scattering factor (ASF), respectively. The ASFs markedly change near absorption edge energy, and they reflect an electronic state attributed to the absorption process. To evaluate the

charge disproportionation of Mn $3d$, $I(E, \vec{Q})$ was measured near the Mn $L_{2,3}$ edge at room temperature. Figure 3(b) shows extremely large intensity modulation near the $L_{2,3}$ edge, while the resonant signal at the Mn K edge is weaker than the Thomson scattering component (Fig. 3(a)) [24]. The intensity is normalized by the non-resonant intensity to compare the strength of the resonant signals [25]. Moreover, there is a large difference between the $I(E, \vec{Q})$ for the two samples; a markedly resonated signal is observed in sample 1. In contrast, a strong resonant signal at the O K edge is observed in sample 2, as shown in Fig. 3(c). The resonating energy is approximately 530 eV, which corresponds to the O $2p$ hole state that reflects the p-d hybridization [26, 27]. The strong single peak structure is similar to the previous reports at the O K edge [16, 17]. These results indicate that the charge disproportionation of O $2p$ is enhanced in sample 2, as expected. It is worth mentioning that the energy spectrum close to the Mn $L_{2,3}$ edge in sample 1 is considerably similar to that in the L2S2 fabricated on a $(LaAlO_3)_{0.3}(SrAl_{0.5}Ta_{0.5}O_3)_{0.7}$ (LSAT) substrate [10]. This is consistent with the fact that L2S2/LSAT shows well insulating behavior.

The energy spectrum $I(E, \vec{Q})$ at the Mn $L_{2,3}$ edge can be calculated on the basis of the Mn $3d$ charge modulation model by utilizing the ASF near the Mn $L_{2,3}$ edge as reported in Ref. [9]. The calculated resonant signal is weaker than the observed one in the case of sample 1. We think that it is caused by the insufficient accuracy of the ASFs at the Mn $L_{2,3}$ edge. There the ASFs of Mn^{3+} and Mn^{4+} were obtained experimentally using reference samples, $LaMnO_3$ and $SrMnO_3$ thin films, respectively. The p-d hybridized states between Mn $3d$ and O $2p$ are not clear in these reference samples. Therefore, the theoretical approach is desired for the quantitative evaluation of the electronic states in the superlattice.

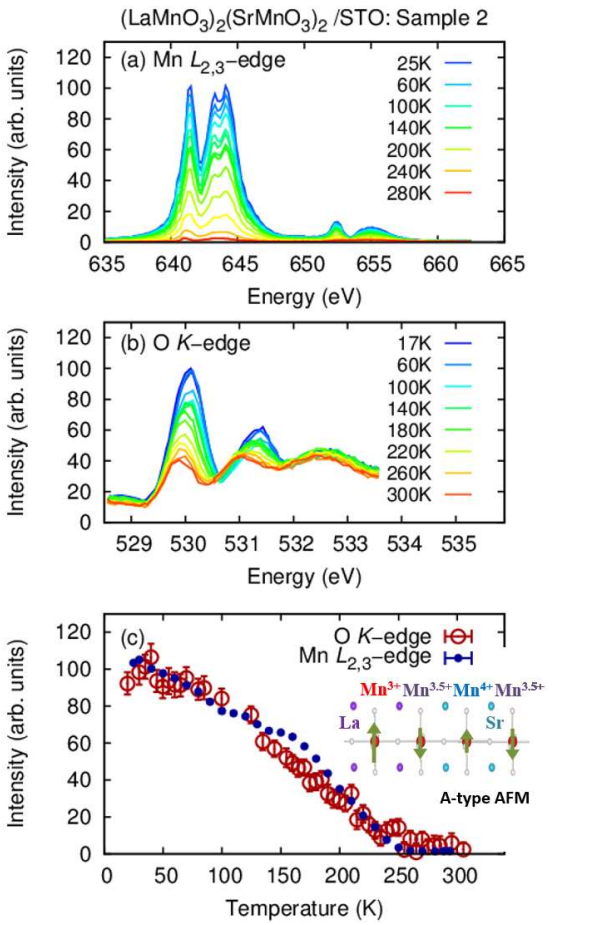

FIG. 4. (Color online) Energy spectra at the (a) Mn $L_{2,3}$ edge and (b) O K edge. (c) Temperature dependence of magnetic scattering intensity at the Mn $L_{2,3}$-edge (641.5 eV) and O K-edge (530 eV). The inset shows schematic view of A-type AFM in L2S2.

Resonant x-ray magnetic scattering

Next, we investigated the magnetic ordering of the superlattices that reflected the p-d hybridized state. A-type antiferromagnetism (AFM) was reported on the manganite film grown on the STO substrate [28, 29]. Reflecting charge disproportionation, the Mn^{3+} ($3d^4$) and Mn^{4+} ($3d^3$) layers have the different moment sizes as shown in the inset of Fig. 4(c), and the periodicity of the magnetic structure coincides with lattice constant c. Namely, the magnetic signal can be expected to appear at the 001 reflection. In theoretical framework, the main component of resonant magnetic scattering is described as $-i(\boldsymbol{\epsilon}' \times \boldsymbol{\epsilon}) \cdot \boldsymbol{S}$, where $\boldsymbol{\epsilon}$ ($\boldsymbol{\epsilon}'$) is polarization vector of incident (scattered) x-ray and $\boldsymbol{S}$ is vector of the magnetic moment [30]. Hence, any magnetic moment can be detected in $\pi \to \pi'$ or $\pi \to \sigma'$ scattering process.

Here the magnetic signal was searched at the 001 reflection in sample 2. The magnetic signal, which was enhanced at low temperature, was clearly found close to the 001 reflection [31], while it was not observed at the 001 reflection in the case of G-type AFM in L2S2/LSAT [10]. Figure 4(a) shows the temperature dependence of energy spectra close to the Mn $L_{2,3}$ edge. The spectra are similar to that of the magnetic signal in the A-type AFM phase of $La_{1.05}Sr_{1.95}Mn_2O_7$ [32]. It indicates that the electronic states of both the A-type AFM phases resemble. Scattering intensity increases at temperatures below approximately 250 K ($= T_N$) (Fig. 4(c)); this corresponds to the magnetization result (Fig. 1(b)). To evaluate oxygen magnetism, which reflects the charge disproportionation of O $2p$, energy spectra were measured close to the O K edge as shown in Fig. 4(b). The intensity at approximately 530 eV is clearly enhanced below T_N. The temperature dependence mostly coincides with that at the Mn $L_{2,3}$ edge (Fig. 4(c)). Hence, magnetic signals with the same origin are detected at the Mn $L_{2,3}$ edge

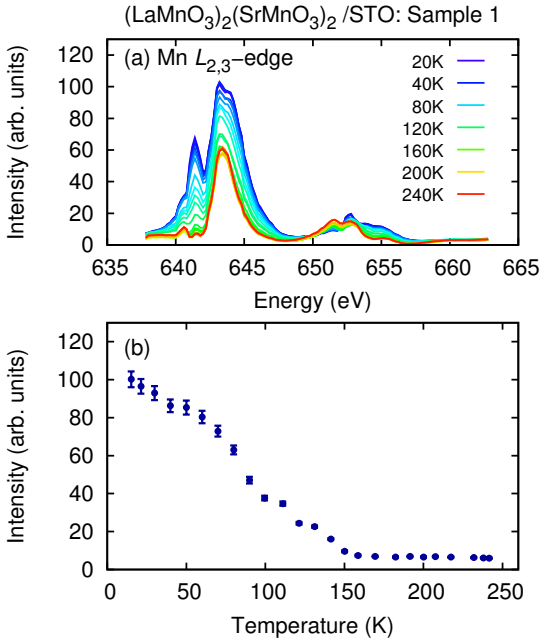

FIG. 5. (Color online) (a) Energy spectra at the Mn $L_{2,3}$ edge. (b) Temperature dependence of the magnetic scattering intensity at the Mn $L_{2,3}$-edge (641.5 eV).

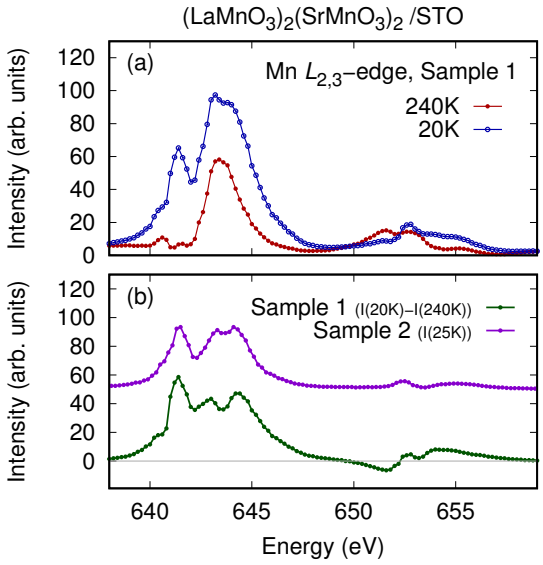

FIG. 6. (Color online) (a) Energy spectra near the Mn $L_{2,3}$ edge at $T = 20$ K and 240 K of sample 1, i.e., $I(20\ \mathrm{K})$ and $I(240\ \mathrm{K})$. (b) Subtracted spectrum, $I(20\ \mathrm{K}) - I(240\ \mathrm{K})$, of sample 1, and the spectrum at 25 K of sample 2. The base of sample 2 is vertically shifted for clarity.

and O K edge.

The magnetism in sample 1 was also investigated. The magnetic signal attributed to A-type AFM is clearly observed at the Mn $L_{2,3}$ edge as shown in Fig. 5(a). Intensity increases below temperatures of approximately 150 K (Fig. 5(b)). The magnetic signal is grown near the signal reflecting the charge disproportionation of Mn $3d$, while the almost pure resonant magnetic signal could be detected for sample 2. To compare the magnetic component of the energy spectrum with that of sample 2, the energy spectrum at 240 K, I (240 K), is subtracted from that at 20 K, $I(20\ \mathrm{K})$, although the magnetic component cannot be simply subtracted from the spectrum owing to the interference. I (240 K), $I(20\ \mathrm{K})$ and the subtracted spectrum are shown in Figs. 6. The subtracted spectrum is similar to the spectrum of sample 2 as shown in Fig. 6(b). It indicates that the A-type AFM phases of sample 1 and 2 have similar electronic states. On the other hand, no magnetic signal is detected at the O K edge in sample 1 within experimental error. Finally, we consider that the O $2p$ magnetism attributed to the charge disproportionation of O $2p$ is clearly observed only in sample 2.

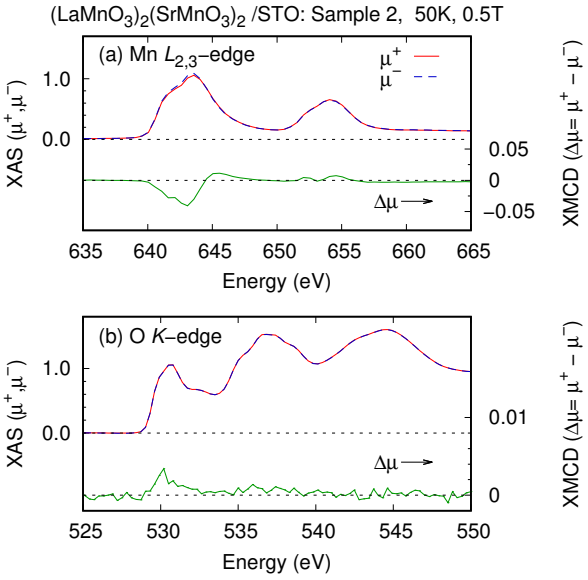

FIG. 7. (Color online) X-ray absorption spectra (XAS) with opposite circular polarizations (μ^+ and μ^-) and XMCD spectrum ($\Delta\mu$) at the (a) Mn $L_{2,3}$ edge and (b) O K edge.

X-ray magnetic circular dichroism

XMCD spectra were measured in sample 2 as slight magnetization was observed as shown Fig. 1(b). Figure 7 shows the XMCD spectrum at the Mn $L_{2,3}$ edge, which is similar to that of the bulk sample [33]. The spectrum was also measured by the FY mode (not shown here), and is consistent with Fig. 7(a). Hence the XMCD spectra reflect not the surface state but the bulk property of the superlattice, although the probing depth in the TEY measurement is much shorter than the film thickness. The XMCD spectrum was also measured at the O K edge. A signal was detected at approximately 530 eV, even

though it was a considerably weak signal. The energy corresponds to that of the magnetic scattering shown in Fig. 4(b). Hence, the O $2p$ magnetism corresponding to the charge disproportionation of O $2p$ can be detected through XMCD at the O K edge. The local magnetic moment at the O site is caused by the charge transfer to the Mn site, hence the moment is simply expected to be antiparallel to that at the Mn site. It is consistent with the positive sign of the XMCD signal at the K edge. However, the opposite sign was also reported in the bulk sample [33]. For detailed understanding, a theoretical study is desired.

Here, we discuss the origin of the charge disproportionation of O $2p$. Sample 2 is expected to have a wider bandwidth compared to sample 1. This is related to the conductivity property in the two samples. The wide bandwidth enhances the p-d hybridization in sample 2, and then, the ligand hole state becomes important. Namely, the $3d^5\underline{L}$ [$3d^4\underline{L}$] state is induced in the Mn^{3+} ($3d^4$) [Mn^{4+} ($3d^3$)] state. It is known that the charge transfer energy of Mn^{3+} is higher than that of Mn^{4+} [34]. As a result, the $3d^4\underline{L}$ state is stabilized compared with the $3d^5\underline{L}$ state. Namely, the Mn^{3+} ($3d^4$) - Mn^{4+} ($3d^4\underline{L}$) type charge disproportionation (Fig. 1(e)) is induced by the p-d hybridization. This is consistent with that the RXS signal at the O K edge is enhanced and that at the Mn $L_{2,3}$ edge is suppressed in sample 2. In addition, we consider the tensile strain effect caused by the STO substrate. The e_g orbital shows energy level splitting, and the x^2-y^2 orbital is stabilized under strain (Fig. 1(f)). Hence, in the case of the charge disproportionation of Mn $3d$, the charge and orbital order can be expected as shown in Fig. 1(d). In the case of the strong p-d hybridization, the $3d(x^2-y^2)\underline{L}$ state has a lower energy level compared to the $3d(3z^2-r^2)\underline{L}$ state under the strain. Therefore, the $3d^4\underline{L}$ state is stabilized furthermore compared with the $3d^5\underline{L}$ state by the tensile strain.

In order to clarify the $3d(x^2-y^2)\underline{L}$ state, XAS spectra at the O K edge of sample 1 and 2 were measured with σ-polarized x rays at room temperature as shown in Fig. 8. In this configuration, the in-plane O $2p$ state can be detected [35], since the polarization vector exists in-plane of the superlattice. The spectra closely resemble that reported in Ref. [13]. The intensity at around 530 eV increases in the sample 2. The energy corresponds to the O $2p$ hole state due to the $p-d$ hybridization [26]. This is consistent with that the $3d(x^2-y^2)\underline{L}$ is enhanced in the sample 2.

CONCLUSION

Through RXS measurements, we have revealed that the charge modulation of the L2S2 superlattice changes from the charge disproportionation of Mn $3d$ to that of O $2p$, accompanying with the conductivity change from insulating to semiconductive. This indicates that L2S2 superlattice is located in the vicinity of MIT and the p-d hybridized states between Mn $3d$ and O $2p$ are changed sensitively by the sample fabrication condition, reflecting the different conductivities in the two samples. In addition, we have elucidated the O $2p$ magnetism attributed to the charge disproportionation of O $2p$. The orbital hybridized state is generally important for clarifying the origin of physical properties in a strongly correlated electron system. In fact, the orbital hybridization between the conduction electron and the f-electron, so called c-f hybridization, is also essential for the physical properties in the rare earth compounds. This study demonstrated that RXS measurement is a key technique to evaluate an order parameter of the orbital hybridized state.

ACKNOWLEDGEMENTS

We wish to thank T. Koide, H. Sagayama, R. Kumai, R. Kadono, and T. Arima for useful discussions. We also thank J. Nishimura, A. Ohtomo, and T. Fukumura for providing us the manganite superlattices. This research was partially supported by JSPS KAKENHI Grant (Nos. 16684008, 21224008, 25286090, JP15H05885 (J-Physics), JP17K05130), the Funding Program for World-Leading Innovative R&D on Science and Technology (FIRST), and the JST, Invitation for Applications for the Strategic Basic Research Programs (CREST). This study has been performed under the Photon Factory Program Advisory Committee (Proposal Nos. 2009S2-008, 2012S2-005, 2015G548, and 2016PF-BL-19B).

* hironori.nakao@kek.jp
† Present address: Institute for Integrated Radiation and Nuclear Science, Kyoto University, Osaka 590-0494, Japan

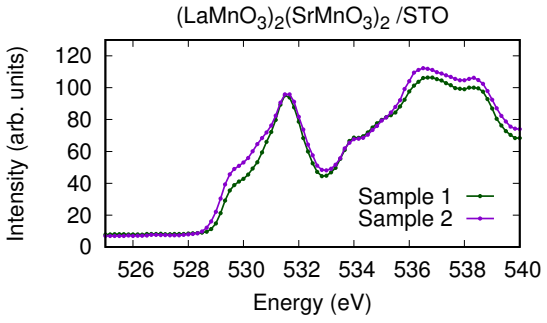

FIG. 8. (Color online) XAS at the O K edge of sample 1 and sample 2. The peak at 531.6 eV is from the STO substrate [13].

[1] M. Imada, A. Fujimori, and Y. Tokura, Rev. Mod. Phys. **70**, 1039 (1998).

[2] J. Zaanen, G. A. Sawatzky, and J. W. Allen, Phys. Rev. Lett. **55**, 418 (1985).

[3] J. B. Torrance, P. Lacorre, A. I. Nazzal, E. J. Ansaldo, and C. Niedermayer, Phys. Rev. B **45**, 8209 (1992).

[4] S. Yamamoto and T. Fujiwara, J. Phys. Soc. Jpn. **71**, 1226 (2002).

[5] T. Koida, M. Lippmaa, T. Fukumura, K. Itaka, Y. Matsumoto, M. Kawasaki, and H. Koinuma, Phys. Rev. B **66**, 144418 (2002).

[6] A. Bhattacharya, S. J. May, S. G. E. te Velthuis, M. Warusawithana, X. Zhai, B. Jiang, J.-M. Zuo, M. R. Fitzsimmons, S. D. Bader, and J. N. Eckstein, Phys. Rev. Lett. **100**, 257203 (2008).

[7] H. Nakao, J. Nishimura, Y. Murakami, A. Ohtomo, T. Fukumura, M. Kawasaki, T. Koida, Y. Wakabayashi, and H. Sawa, J. Phys. Soc. Jpn. **78**, 024602 (2009).

[8] H. Yamada, P.-H. Xiang, and A. Sawa, Phys. Rev. B **81**, 014410 (2010).

[9] M. Kubota, H. Yamada, H. Nakao, J. Okamoto, Y. Yamasaki, A. Sawa, and Y. Murakami, Jpn. J. Appl. Phys. **53**, 05FH07 (2014).

[10] H. Nakao, T. Sudayama, M. Kubota, J. Okamoto, Y. Yamasaki, Y. Murakami, H. Yamada, A. Sawa, and K. Iwasa, Phys. Rev. B **92**, 245104 (2015).

[11] C. Lin, S. Okamoto, and A. J. Millis, Phys. Rev. B **73**, 041104 (2006).

[12] S. Smadici, P. Abbamonte, A. Bhattacharya, X. Zhai, B. Jiang, A. Rusydi, J. N. Eckstein, S. D. Bader, and J.-M. Zuo, Phys. Rev. Lett. **99**, 196404 (2007).

[13] S. Smadici, B. B. Nelson-Cheeseman, A. Bhattacharya, and P. Abbamonte, Phys. Rev. B **86**, 174427 (2012).

[14] T. Beale, G. Beutier, S. Bland, A. Bombardi, L. Bouchenoire, O. Bunau, S. D. Matteo, J. Fernandez-Rodriguez, J. Hamann-Borrero, J. Herrero-Martin, V. Jacques, R. Johnson, A. Juhin, T. Matsumura, C. Mazzoli, A. Mulders, H. Nakao, J. Okamoto, S. Partzsch, A. Princep, V. Scagnoli, J. Strempfer, C. Vecchini, Y. Wakabayashi, H. Walker, D. Wermeille, and Y. Yamasaki, Eur. Phys. J. Special Topics **208**, 89 (2012).

[15] T. Matsumura, H. Nakao, and Y. Murakami, J. Phys. Soc. Jpn. **82**, 021007 (2013).

[16] S. Grenier, K. J. Thomas, J. P. Hill, U. Staub, Y. Bodenthin, M. García-Fernández, V. Scagnoli, V. Kiryukhin, S.-W. Cheong, B. G. Kim, and J. M. Tonnerre, Phys. Rev. Lett. **99**, 206403 (2007).

[17] M. García-Fernández, U. Staub, Y. Bodenthin, V. Scagnoli, V. Pomjakushin, S. W. Lovesey, A. Mirone, J. Herrero-Martín, C. Piamonteze, and E. Pomjakushina, Phys. Rev. Lett. **103**, 097205 (2009).

[18] M. Kawasaki, M. Izumi, Y. Konishi, T. Manako, and Y. Tokura, Mater. Sci. Eng. **63**, 49 (1999).

[19] J. Okamoto, K. Horigane, H. Nakao, K. Amemiya, M. Kubota, Y. Murakami, and K. Yamada, J. Phys.: Conf. Ser. **425**, 202003 (2013).

[20] H. Nakao, Y. Yamasaki, J. Okamoto, T. Sudayama, Y. Takahashi, K. Kobayashi, R. Kumai, and Y. Murakami, J. Phys.: Conf. Ser. **503**, 012015 (2014).

[21] Azimuthal angle dependence and polarization analysis are useful to evaluate a resonant signal. However, these measurements were not performed in this experiment, since the resonant signal at the 001 reflection has only π-π'- scattering component and is invariable by the rotation of azimuthal angle within the tetragonal symmetry. On the other hand, the magnetic signal will indicate azimuthal angle and polarization dependence corresponding to magnetic structure.

[22] K. Amemiya, M. Sakamaki, T. Koide, K. Ito, K. Tsuchiya, K. Harada, T. Aoto, T. Shioya, T. Obina, S. Yamamoto, and Y. Kobayashi, J. Phys.: Conf. Ser. **425**, 152015 (2013).

[23] K. Tsuchiya, T. Shioya, T. Aoto, K. Harada, T. Obina, M. Sakamaki, and K. Amemiya, J. Phys.: Conf. Ser. **425**, 132017 (2013).

[24] RXS spectra at the Mn K edge were also observed at the 003 reflection. $I(E, \vec{Q})$ of two L2S2 samples were almost same as reported in Fig. 15(b) of Ref. [7]. Hence, the sample characteristics are consistent with those reported previously, even though the different piece of sample was used in this experiment.

[25] For quantitative discussion, non-resonant intensity has to be calibrated depending on the 2θ value. Because π-polarized incident x-ray was used in the resonant soft x-ray scattering.

[26] H. L. Ju, H.-C. Sohn, and K. M. Krishnan, Phys. Rev. Lett. **79**, 3230 (1997).

[27] The resonant energy, 530 eV, corresponds with previous reports [13, 26]. However, the resonant energy with about 1-1.5 eV lower was also reported [16, 17]. The difference may be caused by different energy calibration in each beamline.

[28] Y. Konishi, Z. Fang, M. Izumi, T. Manako, M. Kasai, H. Kuwahara, M. Kawasaki, K. Terakura, and Y. Tokura, J. Phys. Soc. Jpn. **68**, 3790 (1999).

[29] S. J. May, P. J. Ryan, J. L. Robertson, J.-W. Kim, T. S. Santos, E. Karapetrova, J. L. Zarestky, X. Zhai, S. G. E. te Velthuis, J. N. Eckstein, S. D. Bader, and A. Bhattacharya, Nat. Mater. **8**, 892 (2009).

[30] J. P. Hannon, G. T. Trammell, M. Blume, and D. Gibbs, Phys. Rev. Lett. **61**, 1245 (1988).

[31] The magnetic signal was observed near the 001 reflection, but not just at the reflection position. It may reflect the step and terrace structure of the substrate, the superlattice periodicity, m, with non-integer value, and so on.

[32] S. B. Wilkins, P. D. Hatton, M. D. Roper, D. Prabhakaran, and A. T. Boothroyd, Phys. Rev. Lett. **90**, 187201 (2003).

[33] T. Koide, H. Miyauchi, J. Okamoto, T. Shidara, T. Sekine, T. Saitoh, A. Fujimori, H. Fukutani, M. Takano, and Y. Takeda, Phys. Rev. Lett. **87**, 246404 (2001).

[34] A. V. Ushakov, S. V. Streltsov, and D. I. Khomskii, J. Phys.: Condens. Matter **23**, 445601 (2011).

[35] C. T. Chen, L. H. Tjeng, J. Kwo, H. L. Kao, P. Rudolf, F. Sette, and R. M. Fleming, Phys. Rev. Lett. **68**, 2543 (1992).